NANO LETTERS

Letter

pubs.acs.org/NanoLett

Fabrication of Broadband Antireflective Plasmonic Gold Nanocone Arrays on Flexible Polymer Films

Mana Toma, Gabriel Loget, and Robert M. Corn*

Department of Chemistry, University of California-Irvine, Irvine, California 92697, United States

Supporting Information

ABSTRACT: Flexible broadband antireflective and light-absorbing nanostructured gold thin films are fabricated by gold vapor deposition onto Teflon films modified with nanocone arrays. The nanostructures are created by the oxygen plasma etching of polystyrene bead monolayers on Teflon surfaces. The periodicity and height of the nanocone arrays are controlled by the bead diameter and the overall etching time. The gold nanocone arrays exhibit a reflectivity of less than 1% over a wide spectral range (450−900 nm) and a wide range of incident angles (0−70°); this unique optical response is attributed to a combination of diffractive scattering loss and localized plasmonic absorption. In addition to nanocones, periodic nanostructures of nanocups, nanopyramids, and nanocavities can be created by the plasma etching of colloidal bilayers. This fabrication method can be used to create flexible nanocone-structured gold thin films over large surface areas (cm^2) and should be rapidly incorporated into new technological applications that require wide-angle and broadband antireflective coatings.

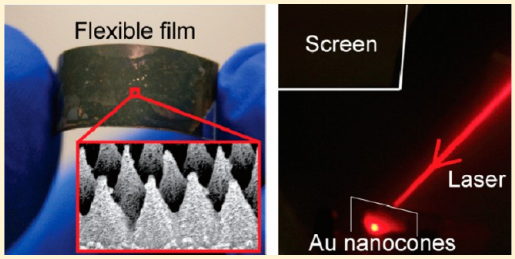

KEYWORDS: *Nanocone, nanosphere lithography, antireflection, black gold, hydrophobic surfaces, Teflon*

Arrays of nanostructures such as nanocones, nanotips, nanopillars and nanowires have attracted great attention recently due to their notable characteristics such as broadband antireflection and light trapping properties,[1−5] strong hydrophobicity[6−8] and high surface area,[9] with applications in photonic[10] and photovoltaic devices,[11] biological and chemical sensors[12] and self-cleaning surfaces.[13] To date, a variety of nanostructures created from metals,[14−16] semiconductors,[5,11,13,17] oxides,[1,3,18] and polymers[4] have been reported. For example, silicon nanostructured arrays are currently studied intensively, as their excellent antireflective properties can provide better efficiency in solar cell applications.[13] Noble metal nanostructured arrays are also studied extensively due to their remarkable mass-transfer properties when used as nanoelectrodes[19] and their notable surface plasmon properties.[20,21] Sharp nanocones and nanotips made with noble metals exhibit strong electromagnetic field enhancement at the tips when they are exposed to a light.[20,21] This plasmonic field enhancement effect has been employed for surface-enhanced Raman spectroscopy,[16,20] surface-enhanced fluorescence,[22] and secondary harmonic generation.[14] The arrays of metal nanostructures also hold a potential as blackbody materials due to their broadband antireflective and light absorption properties, which are induced by the excitation of localized surface plasmon resonances and their interactive coupling.[22−24] Xu et al. fabricated "black silver" by coating the silicone nanocone arrays with a thin silver layer.[22] Søndergaard et al. reported the fabrication of "plasmonic black gold" by creating two-dimensional arrays of sharp convex groove in gold film.[24]

Incorporation of the excellent optical properties of metal nanocone arrays into devices and components requires the development of simple, rapid, and scalable fabrication methods. Serial "top-down" fabrication methods such as focused ion beam etching and e-beam lithography have been used to create metallic nanostructures with precise control.[24,25] However, the fabrication of arrays with these technologies is slow and limited in total obtainable structured area. A parallel "bottom up" approach that combines colloidal lithography and reactive ion etching is an alternative way to fabricate nanocone arrays.[16,22] By using the colloidal monolayer as an etching mask, large scale fabrication of nanocone arrays can be achieved. However, such processes often require multiple etching steps in order to create the desired nanocone structures.

In this paper, we demonstrate a new and very simple fabrication method for creating two-dimensional periodic gold nanocones arrays on flexible Teflon films. In this approach, a combination of colloidal lithography and oxygen plasma etching is employed. The simultaneous competitive differential etching of polystyrene bead layers and Teflon films allows us to fabricate nanocones arrays on the centimeter scale with a single etching step. The periodicity and size of nanocone arrays are easily tuned by changing the bead diameter and the etching time. Unique structures such as nanocups, nanopyramids, nanotips and nanocavities arrays can also be created by applying the same differential etching method to colloid bilayers. After depositing a thin gold layer on top of the nanocone arrays, the surface of nanocone arrays exhibits highly hydrophobic properties and the color of the sample turns

Received: September 18, 2013
Revised: October 29, 2013
Published: November 6, 2013

   dx.doi.org/10.1021/nl403496a | *Nano Lett.* 2013, 13, 6164−6169

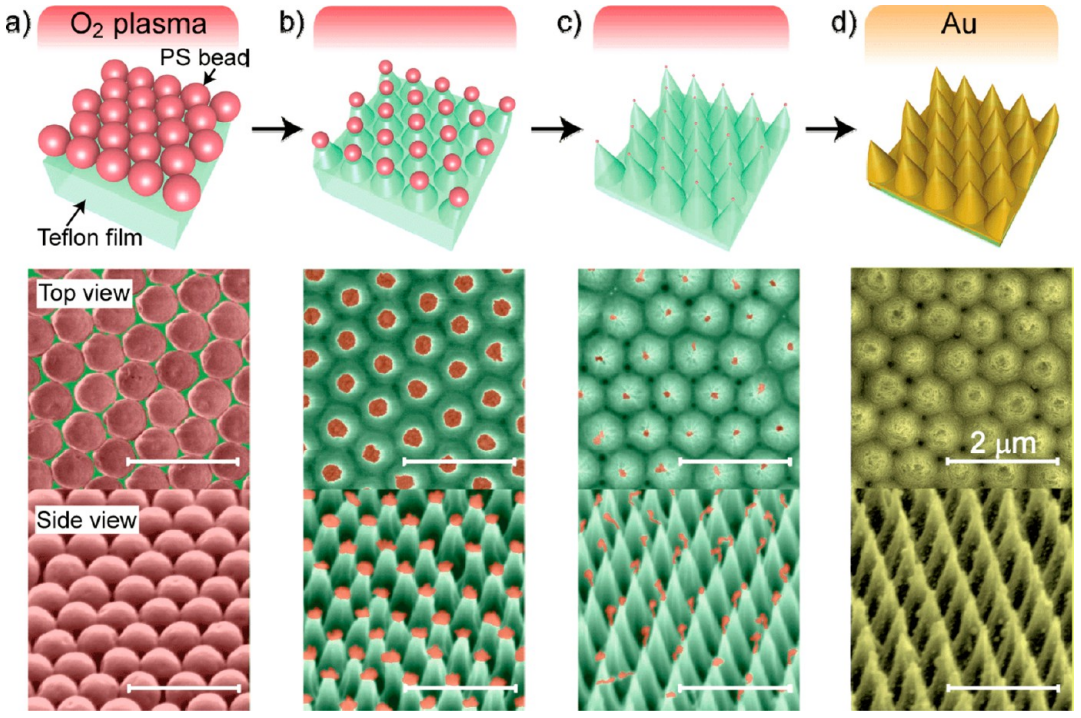

Figure 1. (a–d) Schematic illustration of the fabrication process (top row) and colored SEM images of the corresponding samples in both top (middle row) and tilted (bottom row) views. (a) Fabrication of a PS bead monolayer on a flexible Teflon film. (b,c) Formation of nanocone arrays by simultaneous plasma etching of PS beads and Teflon film. (d) Deposition of gold thin film on the Teflon nanocone array. In all the SEM images, the scalebars indicate 2 μm.

matte-black indicating that the film has acquired broadband antireflection and light absorption properties. Optical measurements reveal that the gold nanocone arrays exhibit low reflectivity (below 1%) and strong absorption (around 90%) at wide angle and wavelength range (450–900 nm).

Fabrication of Nanocone Arrays. The fabrication process of gold nanocone arrays is described in Figure 1. The detailed experimental procedure is provided in Supporting Information. The colored SEM images in middle and bottom rows show the representative samples at each fabrication steps from top and tilted view, respectively. First, a colloidal monolayer is formed on top of flexible Teflon film by spincoating a solution of polystyrene (PS) beads with a diameter of 0.75 μm. After drying the solvent, the PS beads assemble in hexagonal packed arrays on the Teflon film as shown Figure 1a. The surface is then etched by oxygen plasma. During exposure to the oxygen plasma, the PS beads and the Teflon film underneath are etched simultaneously and the nanocone structures are created on the Teflon film (Figure 1b,c). For a short etching time (3 min), a hybrid structure consisting of shrunk PS beads (in pink) and Teflon nanopillars (in green) is created (Figure 1b). As the etching time increases, the PS beads decrease and the heads of nanopillars sharpen. This is illustrated by Figure 1c, obtained for 6 min of etching, which shows that only small PS residues remain on the top of nanocones. Finally, the Teflon nanocones are coated with a thin gold layer (50 nm thick) by thermal evaporation (Figure 1d). As it can be observed on these SEM images, the surface roughness increases after the gold evaporation but the nanocones structure is retained. Figure 2a,b shows photographs of a nanocone array (0.75 μm PS beads, 5 min of oxygen plasma etching) before and after coating of the gold thin film (50 nm thick), respectively. First, one can note that the flexibility of the Teflon film is retained after the fabrication process. Second, the color gives important information about the macroscopic optical properties of these nanostructures. As shown in Figure 2a, due to the formation of the nanocone array the surfaces of Teflon film turns from glossy transparent to matte-white indicating strong light scattering by the nanostructures. The Teflon nanocone array exhibited antireflective property (reflectivity spectrum is shown in Figure S1 in Supporting Information), which is attributed to a gradual effective refractive index changes from air to Teflon.[17] As shown in Figure 2b, the color of the film becomes matte-black after deposition of gold indicating strong light absorption by gold in addition to antireflective property. Moreover, the surface becomes conductive after deposition of gold with a measured conductivity of 22 $mS \cdot cm^{-1}$ which suggests that the gold thin film is continuous over the whole surface. Figure 2c shows an SEM image presenting a large view of gold nanocone arrays. This SEM image reveals that the nanocone array consists of multiple oriented domains of hexagonally packed nanocones. The characteristic dimension of single oriented domains is of several tens of micrometers. Figure 2d shows a photograph of a water drop (10 μL) on the gold nanocone array. The contact angle was measured to be 145°, which is really close to a value of a superhydrophobic surface, 150°. This indicates that the structure of nanocone arrays makes the surface highly hydrophobic in contrast to a plane gold surface (the measured contact angle is 52°) due to the air pockets trapped in the interspaces among nanocones. This structural hydrophobicity of nanocone arrays agrees with the previous works reported by other groups.[7] The array structure in a single domain was studied by the atomic force microscopy (AFM) measurement shown in Figure 2e. This AFM image reveals the hexagonally packed nanocones have a homogeneous height of about 1 μm.

dx.doi.org/10.1021/nl403496a | *Nano Lett.* 2013, 13, 6164–6169

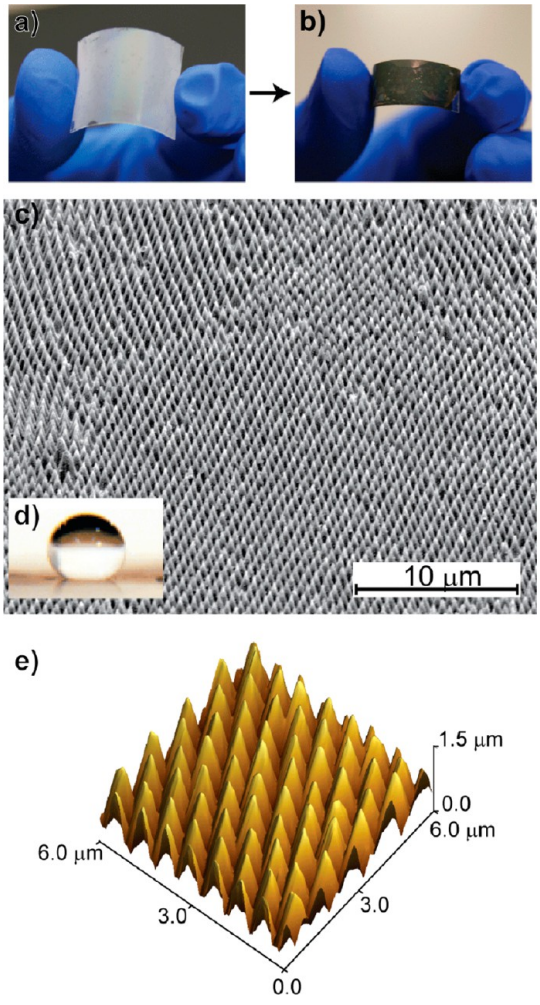

Figure 2. Photographs of the nanocone arrays on Teflon film (a) before and (b) after coating with 50 nm thick gold layer. (c) SEM image of the gold nanocone array in tilted view. (d) Photograph of a water droplet on gold nanocone array showing the hydrophobicity of the surface. (e) Three-dimensional AFM image of the gold nanocone array.

The geometry of the nanocone arrays was controlled by changing the size of PS beads. Figure 3a–d shows the SEM images of nanocone arrays created with PS beads with different diameters, 1, 0.75, 0.5, and 0.35 μm, respectively. The tilted large view, the top view and the side view of gold nanocone arrays are presented in top row, bottom left row, and bottom right row, respectively. Let us note that the nanocone arrays were fabricated with the same O_2 plasma etching time and the SEM images of Figure 3 are directly comparable since they were taken with the same magnification. The large tilted views of nanocone arrays clearly show the significant changes in their dimensions and surface densities depending on the bead diameter. The period of the arrays was obtained from the top view SEM images by fast Fourier transform (FFT) analysis. The heights of nanocones were determined by AFM measurements, shown in Figure S2 in Supporting Information. The period, height, and aspect ratio of each nanocone arrays are summarized in Table 1. The period and height of nanocone

Table 1. Bead Diameters, Periods of Arrays, Heights, Aspect Ratios and Contact Angles of Nanocones Etched for 6 min

bead diameter [μm]	period [μm]	height [μm]	aspect ratio	contact angle [deg]
1.0	0.86 ± 0.1	1.21 ± 0.1	1.4	130 ± 15
0.75	0.70 ± 0.07	1.01 ± 0.13	1.4	145 ± 2
0.5	0.45 ± 0.04	0.59 ± 0.09	1.3	145 ± 4
0.35	0.32 ± 0.02	0.31 ± 0.05	1.0	154 ± 5

array were found to decrease as the bead diameter decreases. The measured periods are slightly smaller than the expected bead diameter for all samples, which could be explained by the slight difference of bead diameter obtained by dynamic light scattering and SEM measurements. The aspect ratio of nanocones, which is obtained from the height of nanocones divided by the period, was determined to vary from 1.4 to 1.0 with the bead diameter from larger to smaller. The hydrophobic properties of the nanocone surfaces shown in Figure 3 were studied by contact angle measurements and were summarized in Table 1. The results revealed that the surface hydrophobicity was enhanced as bead diameter decreased from 1 to 0.35 μm with contact angles ranging from 130 to 155°. This size effect

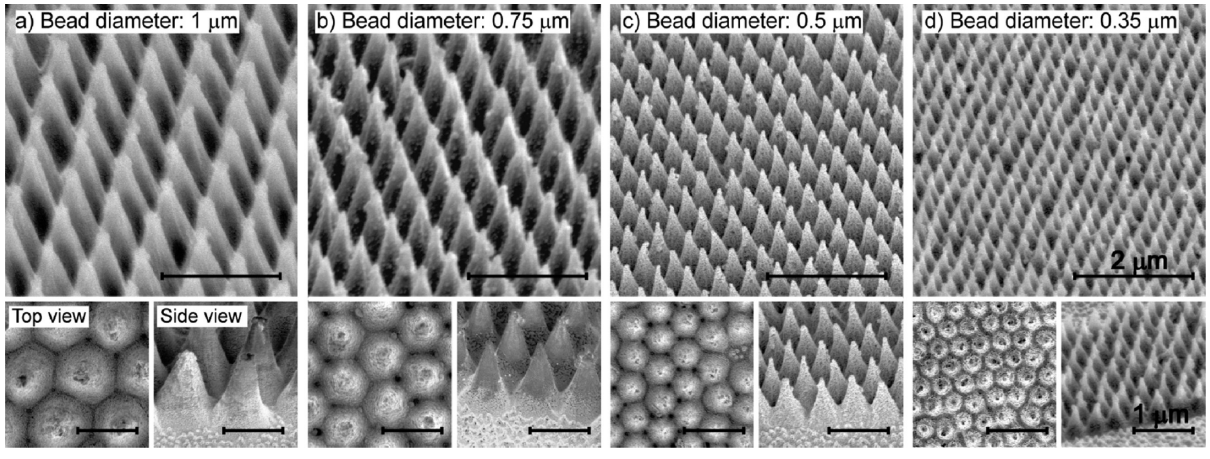

Figure 3. SEM images of nanocone arrays fabricated with PS beads with different diameter (a) 1, (b) 0.75, (c) 0.5, and (d) 0.35 μm. The top row shows large tilted views. In the bottom row, left and right images show top view and side view of nanocones, respectively. In all the top and bottom SEM images, the scalebars indicate 2 and 1 μm, respectively.

dx.doi.org/10.1021/nl403496a | *Nano Lett.* 2013, 13, 6164–6169

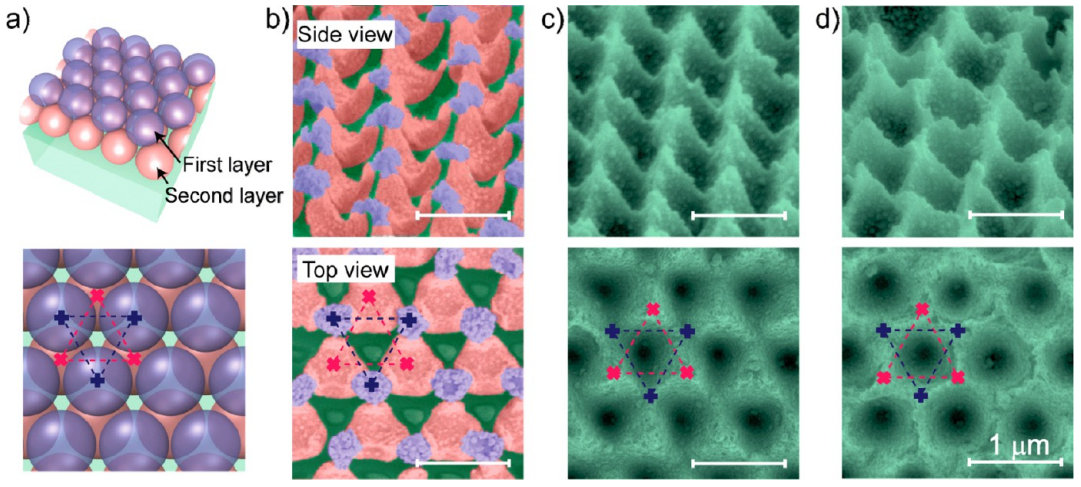

Figure 4. (a) Schematic representation of a colloidal bilayer structure (top, tilted view; bottom, top view). (b–d) Colored SEM images of colloidal bilayer structures after 3, 6, and 12 min O_2 plasma treatment, respectively. The areas corresponding to the first and second PS beads layers and Teflon film are colored following the schematic drawing. In all the SEM pictures, crosses indicate the central position of PS beads at first (blue) and second (magenta) layers and the scalebars indicate 1 μm.

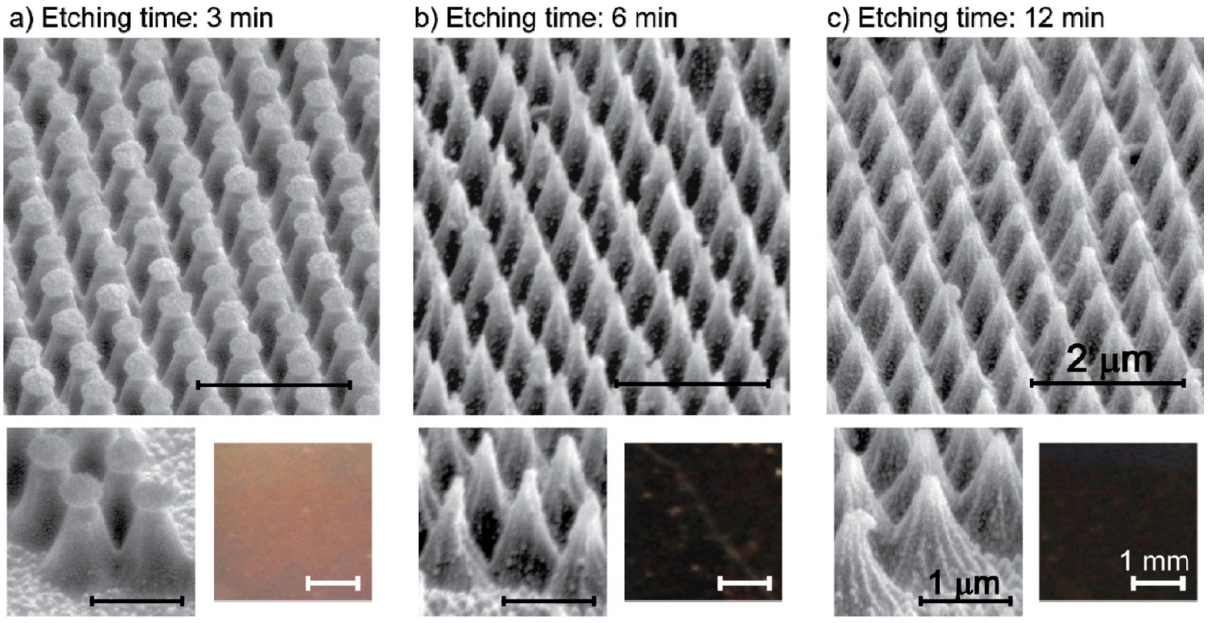

Figure 5. (a–c) SEM images of gold nanocone arrays (top row) and individual nanocones (left figures in bottom row) and photographs of the samples (right figures in bottom row) corresponding to the SEM images that show color of each sample. In all the top SEM images, the scalebars indicate 2 μm and in all the bottom SEM images, the scalebars indicate 1 μm. In all the photographs, the scalebars indicate 1 mm.

can be attributed to the sharpness of the cones and the density of the nanocone arrays.

Fabrication of Complex Structures Using Colloidal Double Layers. In addition to the geometry control of nanocones by the bead diameter, the presented fabrication technique allows us to create more complicated structures such as nanocup, nanopyramid, nanotip, and nanocavity arrays by using bilayers of PS beads. The scheme of a colloidal bilayer structure is shown in Figure 4a. The central positions of PS beads in both top and bottom layers are marked with crosses in the top view image illustrated in bottom row. Figure 4b–d shows colored SEM pictures showing characteristic structures created by using colloidal bilayers (0.75 μm PS beads) with different plasma etching time from 3 to 12 min. For short etching time (3 min), the PS beads in the top layer become smaller but still keep their circular shape, as shown in the top view SEM image in Figure 4b. The PS beads in the bottom layer form a cuplike shape as a result of simultaneous etching of first and second layers of PS beads. The portions of the Teflon film that are not protected with colloids are also etched with triangle shape holes. A similar nanostructure was created by using reactive ion etching of PS beads bilayers by Choi et al.[26] For longer etching time (6 min), the PS beads are totally etched and the Teflon film forms a hybrid structure of nanotriangle pyramids and nanocavity arrays. As marked in Figure 4c, the highest peaks correspond to the center position of the bottom colloidal layer, which are the most protected areas against oxygen plasma. The second peaks correspond to the center of the top colloidal layer. Nanocavities are observed at the center of the triangles made by cross marks where the Teflon film is less protected. When the sample is etched longer

dx.doi.org/10.1021/nl403496a | *Nano Lett.* 2013, 13, 6164–6169

(12 min), the nanopyramids become nanotips and the cavities among nanotips enlarge, as presented by Figure 4d.

Optical Properties of Gold Nanocone Arrays. As we described the fabrication of nanocone arrays and the other structures from a materials science point of view, we now focus on the optical properties of gold nanocone arrays. As briefly mentioned in the previous section, the gold nanocone arrays hold outstanding optical properties which produce their matte-black color (see Figure 2b). First, the color of gold nanocone arrays is controlled by their structure. In the experiment reported in Figure 5, nanocone arrays were fabricated with 0.75 μm PS beads with various oxygen plasma etching times. The fabricated Teflon nanocone arrays were then coated with 50 nm of gold. Figure 5a–c shows the structures and the corresponding colors depending on the plasma etching time: 3, 6, and 12 min. For 3 min plasma etching, the SEM image shows that the colloidal beads are still remained on the top of the cones and the color of the sample is similar to a flat gold film (Figure 5a). As shown in Figure 5b, the color of the sample becomes black with 6 min plasma etching, as the colloidal beads are completely etched and the tips of nanocones get sharper. The color gets slightly brighter for longer etching time (12 min, Figure 5c). This phenomenon is attributed to the lower aspect ratio of nanocones compared to that created by 6 min plasma etching.

Furthermore, we investigated the antireflective properties of gold nanocone arrays prepared with 0.75 μm PS beads and 6 min plasma etching. Figure 6a,b shows the beam path from a

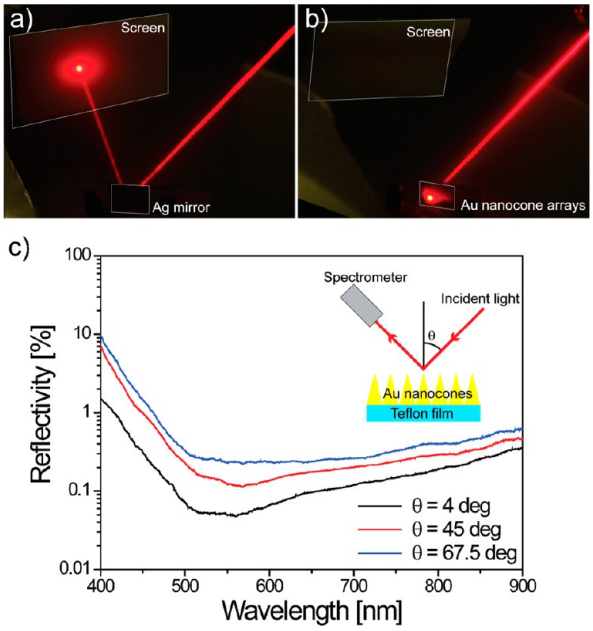

Figure 6. Photographs showing the laser beam path reflected by (a) a silver mirror and (b) a gold nanocone array. (c) Reflectivity spectra from gold nanocone arrays at different angles of incidence, 4° (black), 45° (red), and 67.5° (blue). The inserted schematic shows the optical setup used for reflectivity measurement.

He–Ne laser with a wavelength of 633 nm made incident on and reflected by a flat silver mirror (200 nm thickness) and gold nanocone arrays, respectively. In the case of a gold nanocone array, the photograph clearly shows that almost no light is reflected and no spot is observed on the screen in contrast with the flat silver film that exhibit strong reflection. The wavelength reflectivity spectra from gold nanocone arrays at several angles of incident θ, 4, 45, and 67.5° are presented in Figure 6c. The reference spectrum was taken with a silver mirror. When the angle of incident is set to 4°, the reflectivity R from the gold nanocone array is below 1% at whole wavelength range. The minimum reflectivity R_{min} = 0.05% is observed in a wavelength range between 500 to 550 nm. At 633 nm wavelength, the reflectivity R = 0.1% and transmittance T = 8% (the transmittance spectrum at normal incident is shown in Supporting Information Figure S3). By using a simple equation to determine the absorbance A ($A = 1 - R - T$), it is calculated that the gold nanocone array absorbs over 90% of incident light at this wavelength. Even though the reflectivity slightly increases as the angle of incident increases, the reflectance is kept below 1% for almost whole visible spectrum range above 480 nm in wavelength. Reflectivity measurements were performed on the gold nanocone surfaces obtained with PS beads having different diameters from 0.35 to 1 μm (presented in Figure 3) at normal incident (θ = 4°) and showed similar broadband antireflective properties; those data are shown in Supporting Information (Figure S4). This black coloring is attributed to a combination of diffractive scattering loss from the periodic structure and localized plasmonic absorption from the rough gold film (see Figure 1d).[23] Compared to other metallic nanostructures proposed for antireflective black silver[22] and black gold,[24] our gold nanocone arrays exhibit excellent antireflective properties with a lower reflectance at a visible wavelength range.

In conclusion, we have presented a simple two step method for the fabrication of gold nanocone arrays on flexible films that exhibit excellent broadband antireflective and light absorption properties as well as high hydrophobicity. The nanocone structures were fabricated by the simultaneous oxygen plasma etching of polystyrene colloidal monolayers and the underlying Teflon film. We showed that the periodicity and height of nanocone arrays were tunable with the size of colloid and oxygen plasma etching time. Various unique two-dimensional arrays with structures including nanocups, nanopyramids and nanotips and nanocavities arrays could also be created by etching colloidal bilayers. After deposition of a thin gold film, the nanocone arrays acquire strong black coloring. Reflectivity measurements revealed that the gold nanocone arrays are strongly antireflective (reflectivity below 1%) through the entire visible spectrum and over a wide range of incident angles (0–70°). The flexible nature of these films and the ability to fabricate nanocone arrays on large areas opens up new technologic applications for these wide-angle and broadband antireflective coatings. The strong absorptive properties of the gold nanocone arrays also suggests their potential application in plasmonic blackbody[23] and photovoltaic devices.[27] In the future, we plan to explore the application of nanocone arrays as superhydrophobic and antibactericidal surfaces.[28]

■ ASSOCIATED CONTENT

Supporting Information

The experimental procedure, the reflectivity spectra, AFM measurements, and the transmittance spectrum. This material is available free of charge via the Internet at http://pubs.acs.org.

■ AUTHOR INFORMATION

Corresponding Author

*E-mail: rcorn@uci.edu.

Author Contributions

The manuscript was written through contributions of all authors. All authors have given approval to the final version of the manuscript.

Notes

The authors declare no competing financial interest.

■ ACKNOWLEDGMENTS

The authors thank the laboratory for electron and X-ray instrumentation (LEXI) for the use of the SEM and the plasma cleaner as well as Professor R. M. Penner for the use of his AFM. This work was supported by the NSF Grant CHE-1057638.

■ REFERENCES

(1) Lee, Y.-J.; Ruby, D. S.; Peters, D. W.; McKenzie, B. B.; Hsu, J. W. P. *Nano Lett.* **2008**, *8*, 1501−1505.
(2) Huang, Y.-F.; Chattopadhyay, S.; Jen, Y.-J.; Peng, C.-Y.; Liu, T.-A.; Hsu, Y.-K.; Pan, C.-L.; Lo, H.-C.; Hsu, C.-H.; Chang, Y.-H.; Lee, C.-S.; Chen, K.-H.; Chen, L.-C. *Nat. Nanotechnol.* **2007**, *2*, 770−774.
(3) Tang, Y.-H.; Huang, M.-J.; Su, J.-Y.; Shiao, M.-H. *Jpn. J. Appl. Phys.* **2012**, *51*, 06FF06.
(4) Brunner, R.; Keil, B.; Morhard, C.; Lehr, D.; Draheim, J.; Wallrabe, U.; Spatz, J. *Appl. Opt.* **2012**, *51*, 4370−4376.
(5) Garnett, E.; Yang, P. *Nano Lett.* **2010**, *10*, 1082−1087.
(6) Su, R.; Liu, H.; Kong, T.; Song, Q.; Li, N.; Jin, G.; Cheng, G. *Langmuir* **2011**, *27*, 13220−13225.
(7) D'Urso, B.; Simpson, J. T.; Kalyanaraman, M. *Appl. Phys. Lett.* **2007**, *90*, 044102−3.
(8) Hang, T.; Hu, A.; Ling, H.; Li, M.; Mao, D. *Appl. Surf. Sci.* **2010**, *256*, 2400−2404.
(9) Tiwari, J. N.; Chen, T.-M.; Pan, F.-M.; Lin, K.-L. *J. Power Sources* **2008**, *182*, 510−514.
(10) Fujii, T.; Gao, Y.; Sharma, R.; Hu, E. L.; DenBaars, S. P.; Nakamura, S. *Appl. Phys. Lett.* **2004**, *84*, 855−857.
(11) Chen, Y.; Xu, Z.; Gartia, M. R.; Whitlock, D.; Lian, Y.; Liu, G. L. *ACS Nano* **2011**, *5*, 8002−8012.
(12) Yang, M.; Qu, F.; Lu, Y.; He, Y.; Shen, G.; Yu, R. *Biomaterials* **2006**, *27*, 5944−5950.
(13) Zhu, J.; Hsu, C.-M.; Yu, Z.; Fan, S.; Cui, Y. *Nano Lett.* **2009**, *10*, 1979−1984.
(14) Kontio, J. M.; Husu, H.; Simonen, J.; Huttunen, M. J.; Tommila, J.; Pessa, M.; Kauranen, M. *Opt. Lett.* **2009**, *34*, 1979−1981.
(15) Jiang, Y.; Meng, F.; Qi, D.; Cai, P.; Yin, Z.; Shao, F.; Zhang, H.; Boey, F.; Chen, X. *Small* **2013**, *9*, 2260−2265.
(16) Horrer, A.; Schäfer, C.; Broch, K.; Gollmer, D. A.; Rogalski, J.; Fulmes, J.; Zhang, D.; Meixner, A. J.; Schreiber, F.; Kern, D. P.; Fleischer, M. *Small* **2013**, DOI: 10.1002/smll.201300449.
(17) Zhu, J.; Yu, Z.; Burkhard, G. F.; Hsu, C.-M.; Connor, S. T.; Xu, Y.; Wang, Q.; McGehee, M.; Fan, S.; Cui, Y. *Nano Lett.* **2008**, *9*, 279−282.
(18) Chovin, A.; Garrigue, P.; Vinatier, P.; Sojic, N. *Anal. Chem.* **2004**, *76*, 357−364.
(19) Li, H.; Wu, N. *Nanotechnology* **2008**, *19*, 275301.
(20) Hu, Y. S.; Jeon, J.; Seok, T. J.; Lee, S.; Hafner, J. H.; Drezek, R. A.; Choo, H. *ACS Nano* **2010**, *4*, 5721−5730.
(21) Stade, F.; Heeren, A.; Fleischer, M.; Kern, D. P. *Microelectron. Eng.* **2007**, *84*, 1589−1592.
(22) Xu, Z.; Chen, Y.; Gartia, M. R.; Jiang, J.; Liu, G. L. *Appl. Phys. Lett.* **2011**, *98*, 241904−3.
(23) Kravets, V. G.; Schedin, F.; Grigorenko, A. N. *Phys. Rev. B* **2008**, *78*, 205405.
(24) Sondergaard, T.; Novikov, S. M.; Holmgaard, T.; Eriksen, R. L.; Beermann, J.; Han, Z.; Pedersen, K.; Bozhevolnyi, S. I. *Nat. Commun.* **2012**, *3*, 969.
(25) De Angelis, F.; Malerba, M.; Patrini, M.; Miele, E.; Das, G.; Toma, A.; Zaccaria, R. P.; Di Fabrizio, E. *Nano Lett.* **2013**, *13*, 3553−3558.
(26) Choi, D.-G.; Yu, H. K.; Jang, S. G.; Yang, S.-M. *J. Am. Chem. Soc.* **2004**, *126*, 7019−7025.
(27) Pillai, S.; Catchpole, K. R.; Trupke, T.; Green, M. A. *J. Appl. Phys.* **2007**, *101*, 093105−8.
(28) Pogodin, S.; Hasan, J.; Baulin, V. A.; Webb, H. K.; Truong, V. K.; Phong Nguyen, T. H.; Boshkovikj, V.; Fluke, C. J.; Watson, G. S.; Watson, J. A.; Crawford, R. J.; Ivanova, E. P. *Biophys. J.* **2013**, *104*, 835−840.